The EMBO Journal (2010) 29, 2368–2380 | © 2010 European Molecular Biology Organization | Some Rights Reserved 0261-4189/10
www.embojournal.org

THE EMBO JOURNAL

EMBO open

The C-terminal α–α superhelix of Pat is required for mRNA decapping in metazoa

Joerg E Braun[1], Felix Tritschler[1], Gabrielle Haas, Cátia Igreja, Vincent Truffault, Oliver Weichenrieder* and Elisa Izaurralde*

Department of Biochemistry, Max Planck Institute for Developmental Biology, Tübingen, Germany

Pat proteins regulate the transition of mRNAs from a state that is translationally active to one that is repressed, committing targeted mRNAs to degradation. Pat proteins contain a conserved N-terminal sequence, a proline-rich region, a Mid domain and a C-terminal domain (Pat-C). We show that Pat-C is essential for the interaction with mRNA decapping factors (i.e. DCP2, EDC4 and LSm1–7), whereas the P-rich region and Mid domain have distinct functions in modulating these interactions. DCP2 and EDC4 binding is enhanced by the P-rich region and does not require LSm1–7. LSm1–7 binding is assisted by the Mid domain and is reduced by the P-rich region. Structural analysis revealed that Pat-C folds into an α–α superhelix, exposing conserved and basic residues on one side of the domain. This conserved and basic surface is required for RNA, DCP2, EDC4 and LSm1–7 binding. The multiplicity of interactions mediated by Pat-C suggests that certain of these interactions are mutually exclusive and, therefore, that Pat proteins switch decapping partners allowing transitions between sequential steps in the mRNA decapping pathway.

The EMBO Journal (2010) **29,** 2368–2380. doi:10.1038/emboj.2010.124; Published online 11 June 2010
Subject Categories: RNA
Keywords: DCP1; DCP2; decapping; mRNA decay; P-bodies

Introduction

Decapping of bulk mRNA in eukaryotes occurs after they have been deadenylated. This order of events (deadenylation first, then decapping) ensures that functional, fully polyadenylated mRNAs are not decapped and degraded prematurely (Bail and Kiledjian, 2006; Simon *et al*, 2006; Franks and Lykke-Andersen, 2008). How decapping and deadenylation are coordinated is, however, poorly understood. The yeast protein Pat1 and its orthologs in *Drosophila melanogaster* (HPat) and humans (PatL1) are conserved decapping activators that likely mediate this coordination by interacting both with components of the CAF1-CCR4-NOT1 deadenylase complex and with decapping factors (e.g. the DEAD-box protein Me31B, the decapping enzyme DCP2 and the LSm1–7 ring; Hatfield *et al*, 1996; Bonnerot *et al*, 2000; Bouveret *et al*, 2000; Tharun *et al*, 2000; He and Parker, 2001; Tharun and Parker, 2001; Chowdhury *et al*, 2007; Chowdhury and Tharun, 2008, 2009; Tharun, 2009; Haas *et al*, 2010).

Pat proteins are characterized by a conserved N-terminal sequence of about 50 residues (N-term) followed by a proline-rich region (P-rich), a middle (Mid) domain, and a C-terminal domain termed Pat-C (Figure 1A). Studies in *D. melanogaster* showed that the HPat N-term sequence confers binding to the DEAD-box protein Me31B (*Saccharomyces cerevisiae* Dhh1 and human DDX6/RCK), whereas the Mid domain is necessary and sufficient for LSm1–7 binding (Haas *et al*, 2010). Despite conservation, the N-term sequence is not required to restore decapping in cells depleted of endogenous HPat (Haas *et al*, 2010). In contrast, the P-rich region together with the Mid domain and Pat-C are all required to restore decapping in complementation assays (Haas *et al*, 2010). A somewhat different picture has emerged from studies in *S. cerevisiae* where only the Mid domain was shown to be essential for Pat1 function *in vivo* (Pilkington and Parker, 2008). These differences raise important and unresolved questions: what are the functions of the Pat protein domains in decapping and to what extent are these functions conserved?

In this study, we characterized PatL1, the human ortholog of the Pat protein family. We found that PatL1 interacts with DDX6/RCK, DCP2, EDC4 and the LSm1–7 ring. With the exception of DDX6, these interactions require Pat-C. Moreover, Pat-C is also critical for PatL1 to accumulate in P-bodies and to be incorporated into active decapping complexes. To shed light on the molecular basis for Pat-C functions, we determined the Pat-C three-dimensional structure at 3.1 Å resolution. Pat-C adopts an α–α superhelical fold related to armadillo- and huntigton-elongation-A-subunit-TOR (HEAT)-repeat proteins. Using structure-based mutagenesis, we show that both a basic surface patch and a partially overlapping surface composed of highly conserved residues have a critical function in the interaction with DCP2, EDC4 and the LSm1–7 ring. We further show that the conserved surface of Pat-C is also essential for LSm1–7 binding in *D. melanogaster*. Accordingly, a *D. melanogaster* HPat protein carrying mutations in the conserved Pat-C surface cannot rescue decapping in cells depleted of endogenous HPat. Our results provide structural insight into Pat proteins and show

*Corresponding authors. O Weichenrieder or E Izaurralde, Department of Biochemistry, Max Planck Institute for Developmental Biology, Spemannstrasse 35, 72076 Tübingen, Germany.
Tel.: +49 7071 601 1350; Fax: +49 7071 609 1353
E-mails: oliver.weichenrieder@tuebingen.mpg.de or elisa.izaurralde@tuebingen.mpg.de
[1]These authors contributed equally to this work

Received: 8 April 2010; accepted: 14 May 2010; published online: 11 June 2010

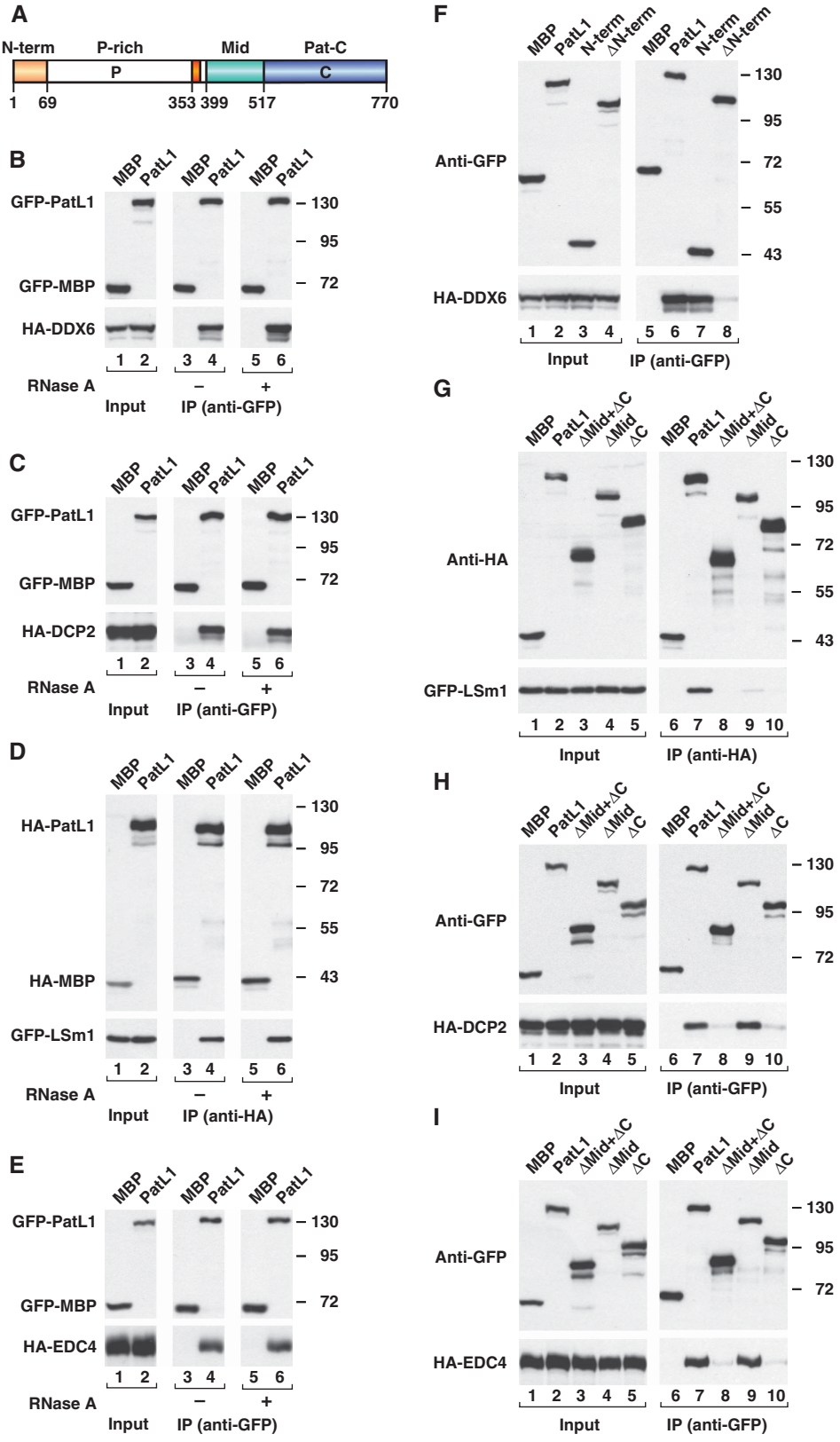

Figure 1 PatL1 coimmunoprecipitates DDX6/RCK, LSm1, DCP2 and EDC4. (**A**) Pat proteins contain a conserved N-term sequence, a P-rich region, a Mid domain and Pat-C. Amino-acid positions at fragment boundaries are indicated for human PatL1. Red box: conserved sequence motif in the P-rich region. (**B–I**) GFP- and HA-tagged proteins were coexpressed in human cells as indicated. Cell lysates were immunoprecipitated using anti-GFP or anti-HA antibodies. GFP- or HA-tagged maltose binding protein (MBP) served as a negative control. In lanes 5–6 of (**B–E**), cell lysates were treated with RNase A before immunoprecipitation. Inputs and immunoprecipitates were analysed by western blotting using anti-GFP and anti-HA antibodies.

that Pat-C has an unprecedented and essential function in mRNA decapping.

Results

PatL1 interacts with DDX6/RCK, DCP2, EDC4 and the LSm1–7 ring

To investigate the function of PatL1 in decapping, we first examined its association with decapping activators in human embryonic kidney 293 cells (HEK293 cells). We observed that epitope-tagged PatL1 coimmunoprecipitated DDX6/RCK, DCP2, LSm1 and EDC4. These interactions were all insensitive to RNase A treatment (Figure 1B–E). Together with earlier studies, these results indicate that Pat proteins establish conserved interactions with DDX6/RCK, DCP2 and the LSm1–7 ring, as these interactions are observed for the orthologous proteins in human, *D. melanogaster*, and *S. cerevisiae* cells (Figure 1B–D; Bonnerot *et al*, 2000; Bouveret *et al*, 2000; Fromont-Racine *et al*, 2000; Tharun *et al*, 2000; Coller *et al*, 2001; Tharun and Parker, 2001; Fischer and Weis, 2002; Haas *et al*, 2010). In contrast, an interaction between Pat proteins and EDC4 has not been reported earlier. This interaction may only occur in metazoa, because there is no EDC4 ortholog in yeast.

Pat-C is the only structured domain in Pat proteins

Pat proteins contain a conserved N-term sequence, the P-rich region, the Mid domain and Pat-C (Figure 1A). Secondary structure predictions suggest that PatL1 residues 1–398 (spanning the N-term sequence and the P-rich region) do not contain a folded protein domain, consistent with the very high content of proline residues (16.4%) and the low level of sequence conservation in the P-rich region.

The two remaining domains (Mid: residues 399–516, and Pat-C: residues 517–770) are well conserved and predicted to be mainly α-helical (Supplementary Figure S1). Using multi-angle static laser-light scattering coupled with size-exclusion chromatography, we found that purified recombinant Pat-C is monomeric in solution (Supplementary Table S1) and elutes as expected for a well behaved, globular protein domain of the respective mass (29 kDa; Supplementary Table S1). A protein fragment containing the Mid domain and Pat-C (residues 399–770) was also monomeric in solution, but eluted much earlier than expected for a globular protein (apparent molecular mass of 75 kDa as opposed to the expected value of 42 kDa (Supplementary Table S1)). These results suggest the Mid domain is unstructured in this context. Accordingly, even if the Mid domain was N-terminally extended to include a conserved motif between residues 353 and 370 (Figure 1A, red box), it did not assume any secondary structure in solution, as determined by NMR analysis (Supplementary Figure S2). Although these results do not rule out the possibility that the Mid domain adopts the predicted secondary structure only when bound to a protein partner, they clearly indicate that Pat-C is the only domain in PatL1 that folds independently as ultimately shown through crystal structure analysis (see below).

PatL1 N-terminal sequence confers binding to DDX6/RCK

In earlier studies, we showed that the N-term sequence of *D. melanogaster* HPat confers binding to Me31B (Haas *et al*, 2010). Accordingly, for human PatL1 the conserved N-term sequence was necessary and sufficient for the interaction with DDX6/RCK (Figure 1F). Two observations support this conclusion: (1) deleting the N-term sequence abolished PatL1 interaction with DDX6/RCK (Figure 1F, lane 8) and (2) when fused to GFP, the N-term sequence alone coimmunoprecipitated DDX6/RCK as efficiently as full-length PatL1 (Figure 1F, lane 7). Thus for PatL1, the ability to bind DDX6/RCK is solely embedded in the conserved N-term sequence.

Pat-C is required for binding to DCP2, EDC4 and the LSm1–7 ring

Next, we investigated which domains of PatL1 are required for the interaction with DCP2, EDC4 and the LSm1–7 ring. We observed that PatL1 interaction with LSm1 required both the Mid domain and Pat-C (Figure 1G). Indeed, deleting these domains either individually or in combination abolished LSm1 binding (Figure 1G, lanes 8–10). In contrast, only Pat-C, but not the Mid domain, was required for PatL1 to interact with DCP2 and EDC4 (Figure 1H and I, lanes 9 and 10). An important implication from these results is that DCP2 and EDC4 interact with PatL1 independently of the LSm1–7 ring. Indeed, a PatL1 mutant lacking the Mid domain (ΔMid) no longer interacts with the LSm1–7 ring but retains the ability to associate with DCP2 and EDC4 (Figure 1G–I, lane 9). Furthermore, PatL1 interaction with LSm1, DCP2 or EDC4 was not affected by deleting the N-term sequence (Supplementary Figure S3A–C), indicating that these proteins associate with PatL1 independently of DDX6/RCK. Of note, DCP2 and EDC4 interact with each other (Fenger-Grøn *et al*, 2005; Jínek *et al*, 2008), and may associate with PatL1 as a complex.

The Pat-C and P-rich regions cooperate to bind DCP2 and EDC4

To gain a precise understanding of the sequences in PatL1 important for DCP2 and EDC4 binding, we performed coimmunoprecipitation assays with several PatL1 fragments. As mentioned above, a PatL1 fragment containing the P-rich region, the Mid domain and Pat-C (PatL1-ΔN-term) behaved similar to wild type in binding DCP2 and EDC4 (Supplementary Figure S3A and B). In contrast, without the P-rich region, the Mid domain and Pat-C showed lower affinity to EDC4 and did not bind DCP2 (Figure 2A and B, lane 10). Thus, in addition to Pat-C, the P-rich region is also required for binding EDC4 and DCP2. Accordingly, a protein fragment containing the P-rich region and Pat-C was sufficient for binding to EDC4 and DCP2 (Figure 2A and B, lane 9). These results provide further evidence that EDC4 and DCP2 binding does not require the Mid domain; and thus, this interaction occurs independently of the LSm1–7 ring.

The Mid domain and Pat-C form a bipartite LSm1-binding site

As shown in Figure 1G, deleting Pat-C abrogates LSm1 binding. This result contrasts with earlier studies showing that the Mid domain is sufficient for LSm1 binding both in *S. cerevisiae* and *D. melanogaster* cells (Pilkington and Parker, 2008; Haas *et al*, 2010). Therefore, we investigated further, for the human protein, the contribution of the Mid domain and Pat-C in LSm1 binding. This analysis revealed two unexpected findings: (1) Pat-C, but not the Mid domain, was sufficient for LSm1 binding; although binding was reduced

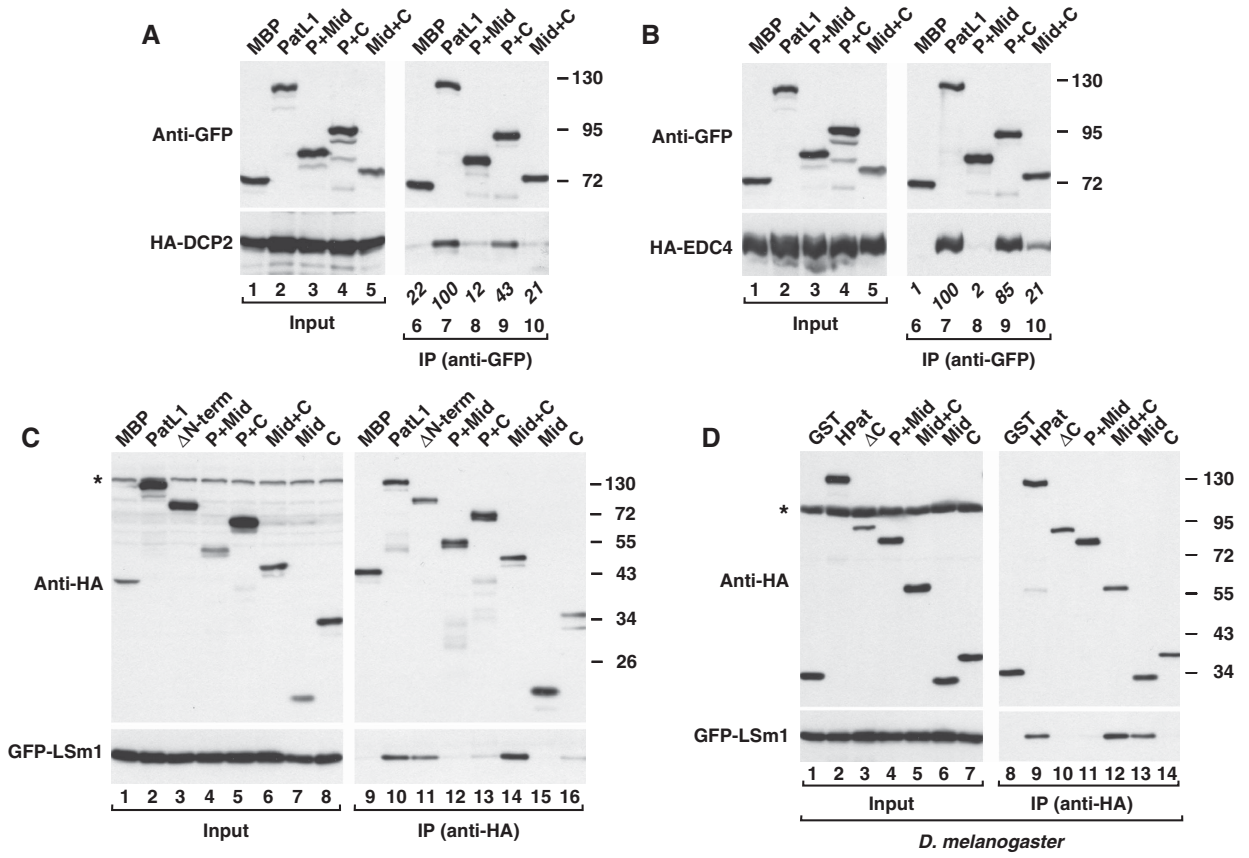

Figure 2 Pat-C is required for binding to DCP2, EDC4 and LSm1–7. (**A–C**) GFP- and HA-tagged proteins were coexpressed in human cells as indicated. Cell lysates were immunoprecipitated using anti-GFP or anti-HA antibodies and analysed as described in Figure 1. Numbers in italics below the lanes in (**A**, **B**) represent coimmunoprecipitation efficiencies relative to wild-type PatL1. Values take into account differences in protein expression levels in the inputs and the relative amount of PatL1 proteins in the immunoprecipitates. (**D**) HA-tagged wild-type HPat and fragments were expressed in *D. melanogaster* S2 cells together with GFP-LSm1. Cell lysates were immunoprecipitated using anti-HA antibodies. Asterisks indicate cross-reactivity of the primary antibodies with an endogenous protein (input panels).

relative to the wild type (Figure 2C, lane 16 versus 10) and (2) in several independent experiments, a fragment containing the Mid domain and Pat-C coimmunoprecipitated LSm1 more efficiently than wild-type PatL1 or PatL1-ΔN-term (Figure 2C, lane 14; Supplementary Figure S3C); these findings suggest that Pat-C and the Mid region cooperate to provide a high-affinity binding site for LSm1. Furthermore, PatL1 must contain sequences that interfere with LSm1 binding because the wild-type protein binds LSm1 less efficiently than a fragment containing the Mid domain and Pat-C. These interfering sequences are located in the P-rich region, because a PatL1 mutant lacking the N-term sequence also showed reduced LSm1 binding (Figure 2C, lane 11). We conclude that the Mid domain and Pat-C provide a bipartite binding site for LSm1–7, and that the P-rich region interferes with this binding.

The P-rich region interferes with LSm1 binding in D. melanogaster

The observations described above prompted us to re-investigate the interaction between HPat and LSm1 in *D. melanogaster*, where we previously showed that the Mid domain was sufficient for LSm1 binding (Haas *et al*, 2010). As reported before (Haas *et al*, 2010), we confirmed that the Mid domain alone, but not Pat-C, was sufficient for LSm1 binding (Figure 2D, lane 13 versus 14). When the Mid domain was fused to Pat-C, the affinity for LSm1 increased slightly, suggesting that Pat-C contributes to the interaction (Figure 2D, lane 12). In contrast, in mutants lacking Pat-C, but containing the Mid domain and the P-rich region, the interaction with LSm1 was abolished (ΔC and P + Mid; Figure 2D, lanes 10 and 11). We conclude that in *D. melanogaster* HPat, the Mid region confers binding to the LSm1–7 ring. This binding is enhanced by Pat-C and inhibited by the P-rich region. The interfering effect of the P-rich region is only observed in the absence of Pat-C, suggesting that Pat-C counteracts the negative effect of the P-rich region. As described above, the negative effect of the P-rich region is less pronounced for human PatL1, most likely because the major LSm1–7-binding site is provided by Pat-C and not by the Mid domain.

Pat-C is required for PatL1 incorporation into active decapping complexes

To investigate which domains of PatL1 are required for the assembly of active decapping complexes, we performed decapping assays *in vitro*. To this end, we immunoprecipitated GFP-PatL1 (wild-type or deletion mutants) from HEK293 cells and, using an m^7G-capped RNA substrate, tested for decapping activity. Immunoprecipitated GFP-PatL1 exhibited decapping activity (Figure 3A, lane 4), whereas a PatL1 mutant lacking the Mid and Pat-C domains did not copurify with decapping activity (Figure 3A, lane 5).

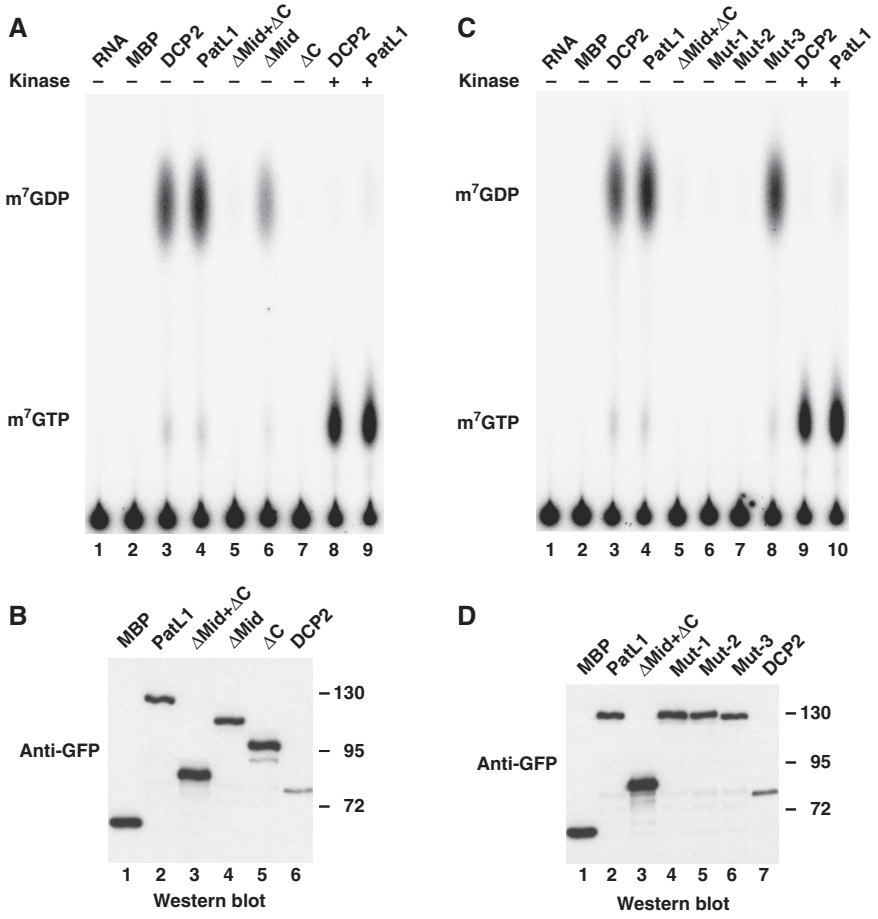

Figure 3 Pat-C is required for PatL1 incorporation into active decapping complexes. (**A**–**D**) GFP-tagged proteins were expressed in human cells. Cell lysates were immunoprecipitated using anti-GFP antibodies. The immunoprecipitates were tested for decapping activity using *in vitro* synthesized ^{32}P-labelled capped mRNA. Samples corresponding to (**A**, **C**) were analysed by western blotting in (**B**, **D**), respectively, to ensure that equivalent amounts of proteins were present in the decapping assay.

Thus, the Mid domain and Pat-C enable PatL1 incorporation into active decapping complexes.

The decapping activity coimmunoprecipitating with PatL1 likely comes from the associated DCP2 (as a positive control, compare an immunoprecipitation of GFP-DCP2; Figure 3A, lane 3). Two observations support this conclusion: (1) if we added nucleotide diphosphate kinase to the decapping reactions containing either PatL1 or DCP2, then the m^{7}GDP product was converted to m^{7}GTP (Figure 3A, lanes 8 and 9; van Dijk *et al*, 2002; Fenger-Grøn *et al*, 2005) and (2) a PatL1 mutant lacking Pat-C, which does not interact with DCP2, did not copurify with decapping activity (Figure 3A, lane 7). In contrast, a mutant carrying a deletion of the Mid domain, which interacts with DCP2 but not with the LSm1–7 ring, was impaired but could still coimmunoprecipitate decapping activity (Figure 3A, lane 6). The amounts of PatL1 mutants in the decapping assay were comparable to those of wild type (Figure 3B). Thus, Pat-C is required for PatL1 association with active decapping complexes.

Pat-C is required for P-body localization

S. cerevisiae Pat1 and its orthologs in metazoa localize to P-bodies and are required for P-body integrity (Scheller *et al*, 2007; Eulalio *et al*, 2007a; Pilkington and Parker, 2008). To define which domains are critical for human PatL1 to localize to P-bodies, we examined the subcellular localization of PatL1 fragments in human cells. GFP-PatL1 localized to endogenous P-bodies (Figure 4A) as judged by the staining with antibodies recognizing EDC4 (Kedersha and Anderson, 2007). A fragment of PatL1 comprising the N-term sequence and P-rich region dispersed throughout the cytoplasm in 96% of cells (Figure 4B). Moreover, 31% of the cells expressing this fragment showed no detectable P-bodies, indicating this protein fragment affects P-body integrity in a dominant-negative manner. In contrast, a protein fragment comprising the Mid domain and Pat-C retained the ability to localize to P-bodies (16% of cells), although much less efficiently than full-length PatL1 (Figure 4C versus 4A).

We next investigated whether the Mid domain or Pat-C are required for PatL1 to localize to P-bodies. A PatL1 mutant lacking the Mid domain was detected in P-bodies in 49% of cells (Figure 4D), suggesting the Mid domain contributes, but is not required for P-body localization. In contrast, a mutant lacking Pat-C spread throughout the cytoplasm in 96% of cells, although EDC4-contaning foci were detectable in 47% of cells (Figure 4E). Together, these results indicate that Pat-C has a critical function in promoting PatL1 accumulation in P-bodies.

Crystal structures of the human Pat-C domain

So far, our data indicate that Pat-C is required for binding to DCP2, EDC4 and LSm1–7 and also enables PatL1 to localize to P-bodies and be incorporated into active decapping complexes. To gain a more detailed understanding of these functions, we determined the crystal structure of Pat-C.

We obtained well-diffracting crystals of Pat-C (residues 517–767) and of Pat-C-Δloop (residues 517–767), where a putative loop (residues 664–673) was replaced by a Gly-Ser linker (Supplementary Figure S1B). Initially, the structure was solved using single anomalous dispersion data (2.2 Å resolution) collected at the absorption peak of a selenomethionine-substituted protein crystal of Pat-C-Δloop. The structure was automatically built starting from an excellent multiple anomalous dispersion electron density map, and was manually refined to an R_{work} of 19.9% (R_{free} = 23.2%), with two molecules per asymmetric unit (crystal form I; Supplementary Table S2; Supplementary Figure S4A).

Subsequently, this model was used in molecular replacement to solve the structure of Pat-C at 3.1 Å resolution, with four molecules per asymmetric unit in a different packing environment (R_{work} = 24.8%, R_{free} = 28.1%, crystal form II; Supplementary Table S2 and Supplementary Figure S4A). Finally, we obtained an unrelated crystal form of Pat-C-Δloop at 2.95 Å resolution (R_{work} = 24.8%, R_{free} = 29.2%, crystal form III; Supplementary Table S2). In this crystal form, two of the three molecules in the asymmetric unit apparently contain a specifically bound sulphate ion from the crystallization condition, coordinated by two arginines (Arg591 and Arg595; Supplementary Figure S4B). Sulphate ions can mimic the phosphate groups of the nucleic acid backbone and therefore indicate potential nucleic acid-binding sites (see below).

Pat-C folds into an α–α superhelix

Pat-C is composed of 13 α-helices, stacked into a superhelix with a right-handed twist. The first two helices are significantly longer than the others and form a hairpin that protrudes ~20 Å from the cylindrical core of the domain, giving Pat-C an overall L-shape (Figure 5A–C).

According to the structural classification of proteins (SCOP; Murzin *et al*, 1995), the α–α superhelix fold (SCOP classification 48370) is a feature of >20 protein superfamilies. Among those, the structure of Pat-C clusters with members of the ARM-repeat superfamily, as revealed by a search using the Dali server (Holm and Sander, 1995). The ARM-repeat superfamily includes families such as the armadillo-, HEAT- and Pumilio-repeat families. The best-scoring structural relatives of Pat-C thus include yeast Cse1 (Matsuura and Stewart, 2004), human Pumilio1 (Wang *et al*, 2002) and interestingly, the C-terminal domain of EDC4 (Jínek *et al*, 2008).

Compared with canonical armadillo-, HEAT- or Pumilio-repeat domains, however, the helical arrangement of Pat-C is

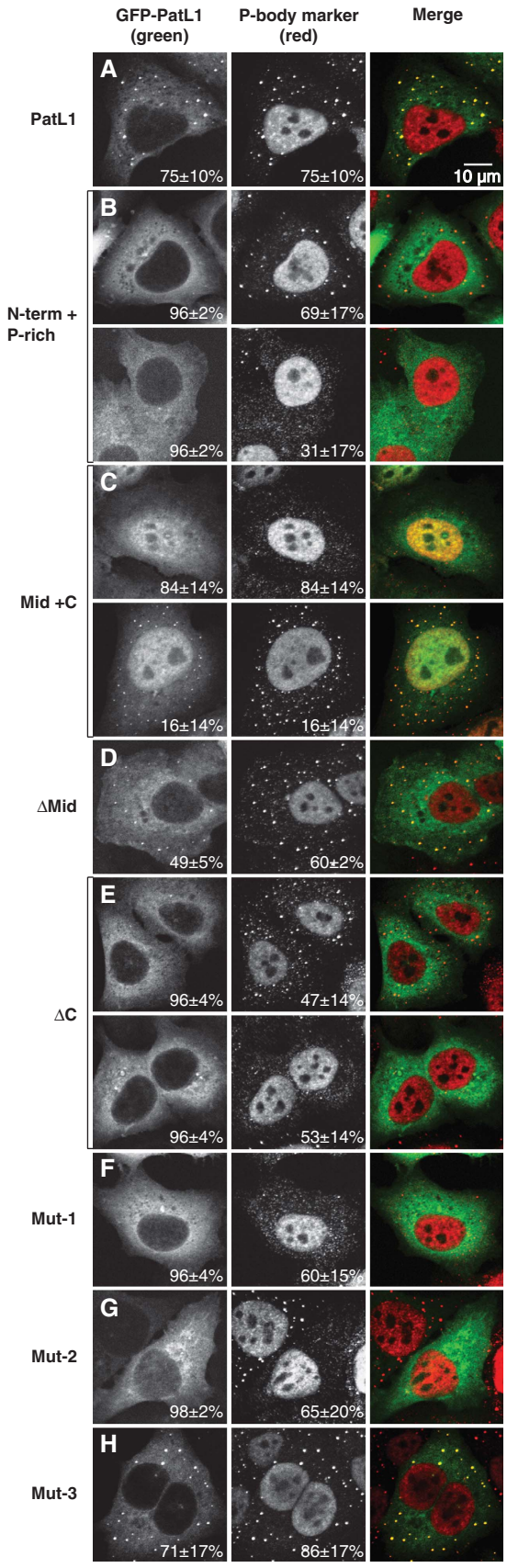

Figure 4 Pat-C is required for PatL1 accumulation in P-bodies. (**A**–**H**) Representative confocal fluorescent micrographs of fixed human HeLa cells expressing wild-type GFP-PatL1 or the mutants indicated on the left. Cells were stained with antibodies cross-reacting with EDC4 and a nuclear human antigen (Kedersha and Anderson, 2007). The merged images show the GFP signal in green and the EDC4 signal in red. The fraction of cells exhibiting a staining identical to that shown in the representative panel was determined by scoring at least 100 cells in each of the three independent transfections performed per protein. Scale bar: 10 μm.

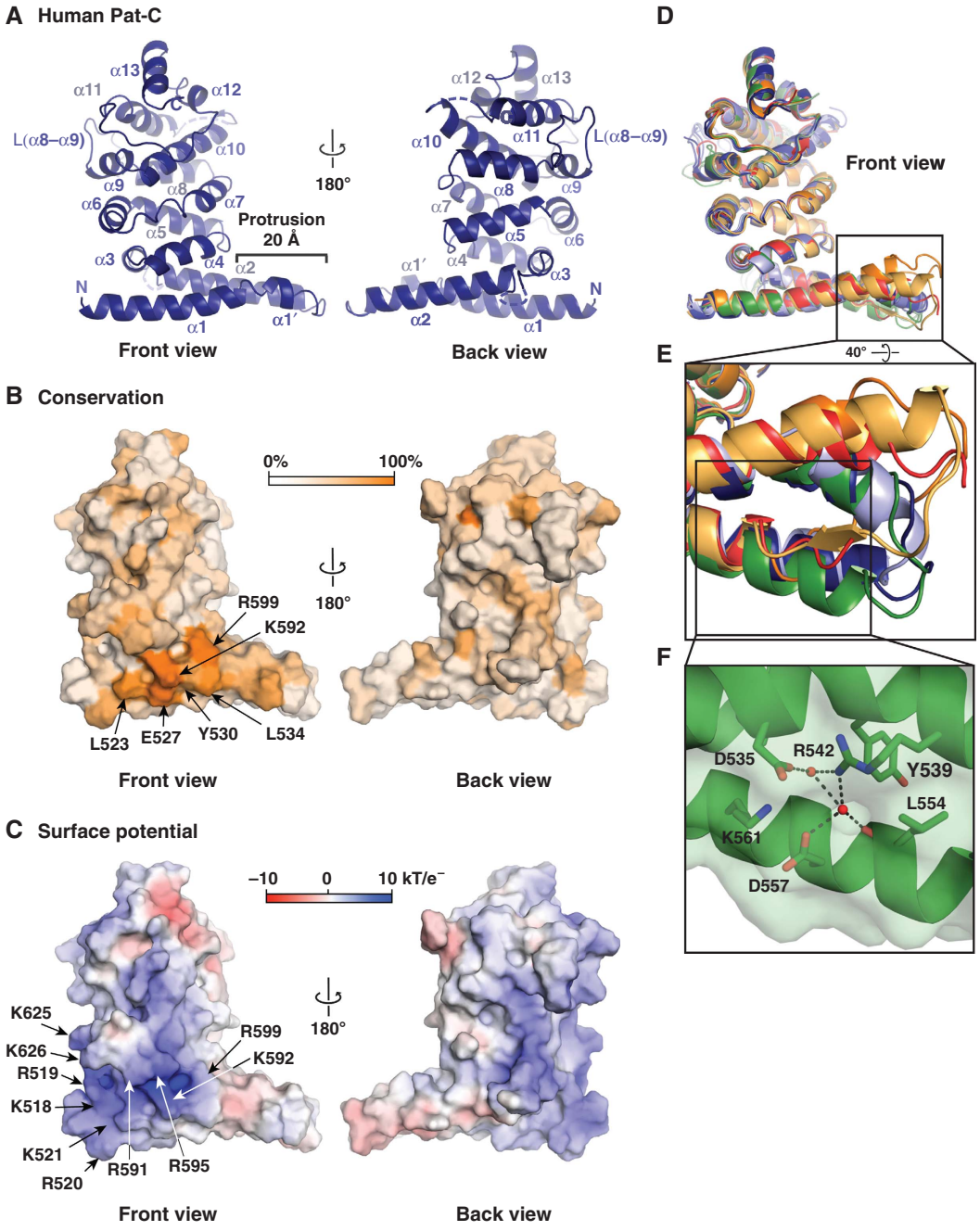

Figure 5 Structure of human Pat-C (Form II, chain A). (**A**) Ribbon diagram in two orientations related by a 180° rotation along a vertical axis. Loop L(α8–α9) is replaced by a Gly-Ser linker in Pat-C-Δ-loop construct. Structural representations were generated using Pymol (http://www.pymol.org). (**B**) Surface representation, coloured by sequence conservation, comparing six species (Supplementary Figure S2B). Colour ramp by identity: orange (100%) to white (0%). Highly conserved solvent exposed residues are labelled. (**C**) Electrostatic potentials are mapped onto the molecular surface of Pat-C and contoured from −10 kT/e$^-$ (red) to 10 kT/e$^-$ (blue). Residues contributing to the positively charged surface patch are labelled. (**D**) Ribbon representation of six Pat-C molecules resulting from the three independent crystal forms. Green (Form I, chain A), dark blue (Form II, chain A), light blue (Form II, chain B), orange (Form III, chain A), red (Form III, chain B), yellow (Form III, chain C). (**E**) Close-up view (40° rotated along a horizontal axis) on the helical protrusion of the six structurally most divergent Pat-C molecules. Colours are as in (**D**). (**F**) Close-up on Form I, chain A, showing two water molecules buried in the helical protrusion. Residues adjacent to the buried water molecules are labelled and shown as sticks with carbons in green, nitrogens in blue and oxygens in red. Hydrogen bonds are shown as dashed lines.

quite irregular and structural alignments of >100 residues consistently yielded C_α root mean square deviations (r.m.s.d.) higher than 2.9 Å. Only the first nine helices (α1–α9) may be classified as ARM-like repeats of three helices each. Furthermore, Pat-C contains three large, partially ordered or disordered loops that cluster on one face of the molecule. These loops are located between helices α2 and α3 (L(α2–α3)), α8 and α9 (L(α8–α9)) and α10 and α11 (L(α10–α11); Figure 5A, back view; and Supplementary Figure S4A).

Aligning the Pat-C sequence across different species shows that key surface and structural residues are highly conserved.

This suggests that Pat-C adopts very similar fold with related functions in all members of the Pat protein family (Supplementary Figure S1B).

The helical protrusion of Pat-C exhibits structural flexibility

The three crystal forms of Pat-C provide nine independent structures, in distinct molecular packing environments. These nine structures superimpose well over the cylindrical core of the domain with an r.m.s.d. of 0.58 Å (excluding loops (L(α2–α3), L(α8–α9) and L(α10–α11); Figure 5D). The helical protrusion, however, displays significant structural variability, especially near the tip of the hairpin (residues 539–557; Figure 5D). The most extreme deviations are found in the structures of crystal form III, with the distal parts of helix α2 (residues 550–558) being melted into an ordered loop (Figure 5E, orange chain), or into an ordered loop with a short β-strand (yellow), or into an entirely disordered loop (red). One reason for this structural variability is likely the hydrophilic nature of residues D535, R542 and D557. Although being exposed to solvent in crystal form III, they are also able to mediate close helix packing in crystal form I, through two deeply buried water molecules (Figure 5F). The structural variability of the helical protrusion suggests a significant flexibility, which might be of functional importance.

A basic surface on Pat-C confers binding to RNA

Proteins with an α–α superhelical fold frequently provide scaffolds for protein or nucleic acid interactions (Huber *et al*, 1997; Edwards *et al*, 2001). In addition to be required for protein–protein interactions, the Pat-C domain of yeast Pat1 shows affinity for RNA (Pilkington and Parker, 2008). We therefore looked for patches of conserved and/or basic residues on the surface of Pat-C that might mediate the observed interactions with decapping factors and/or with RNA. The most highly conserved surface patch on Pat-C is located near the N-terminal end of helix α1, close to the connection to the Mid domain. It shares contributions from Leu523, Glu527, Tyr530 and Leu534 on helix α1 as well as contributions from Lys592 and Arg599 on helix α4 (Figure 5B).

The conserved patch partially overlaps with a region of high positive surface potential (Figure 5C), which coordinates the sulphate ion in crystal form III (Supplementary Figure S4B) and results from a high concentration of positively charged residues (Lys518, Arg519, Arg520, Lys521 on helix α1, Arg591, Lys592, Arg595, Arg599 on helix α4 and Lys625, Lys626 on helix α6). We therefore tested whether Pat-C could bind RNA and found that it directly binds to an U_{30} RNA oligomer in size exclusion chromatography experiments (Supplementary Figure S5A).

In further experiments, we established that Pat-C exhibits RNA-binding properties similar to those reported for the purified yeast Pat1-LSm1–7 complex (Chowdhury *et al*, 2007). For instance, Pat-C interacted with oligo$(rU)_{30}$ but not with oligo$(rA)_{30}$ (Supplementary Figure S5A and F). Similarly, Chowdhury *et al* (2007) showed that yeast Pat1-LSm1–7 complex interacts with oligo(rU) but not with any other homo-oligoribonucleotide. Furthermore, Pat-C interacted with a 30-nucleotide long homo(rU)-oligomer, but failed to interact with oligomers containing 20 and 15 nucleotides (Supplementary Figure S5A–C). Similarly, a requirement that RNA be a minimum length for detectable binding was reported for the purified yeast Pat1-LSm1–7 complex (Chowdhury *et al*, 2007), suggesting that some of the RNA-binding properties of the complex can be attributed to Pat-C. Finally, Pat-C discriminated between ribo- and deoxy-oligoribonucleotides, as it did not interact with 2′-deoxy-oligo$(U)_{30}$ (Supplementary Figure S5F).

To investigate how much the Pat-C conserved and basic patches contribute to RNA and protein binding, we generated three mutants. In mutant 1 (Mut-1), six basic residues in the positively charged patch were substituted with alanines (R519, R520, R591, R595, K625 and K626; Supplementary Figure S1B). In mutant 2 (Mut-2), four residues form the conserved patch were changed into serine or alanine (L523S, E527A, Y530A and L534S; Supplementary Figure S1B). Finally, in mutant 3 (Mut-3), residues 539 to 557 were substituted with a GSGSGSG linker (Supplementary Figure S1B), thus excising the helical protrusion. When expressed, purified and analysed by size exclusion chromatography, all three Pat-C mutants showed the expected elution volumes for folded monomeric proteins of the respective size (Supplementary Table S1), indicating that the mutations do not disrupt the Pat-C fold. Importantly, Mut-1 lost the ability to bind U_{30} RNA, whereas Mut-2 was comparable to the wild-type protein (Supplementary Figure S5D and E). Together, these results indicate that the basic surface on the Pat-C domain confers the ability to bind RNA.

The conserved and basic surfaces on Pat-C are required for binding to DCP2/EDC4 and LSm1–7

We also investigated how the Pat-C conserved and basic patches contribute to the interactions with decapping factors. To this end, we introduced the mutations described above in the context of full-length PatL1 and examined the effect on DCP2, LSm1–7, and EDC4 binding, as well as on decapping and P-body localization. We found that mutations in the basic and conserved patches (Mut-1 and Mut-2) prevented PatL1 from interacting with DCP2, EDC4 and the LSm1–7 ring as efficiently as deleting the Mid and Pat-C domains (Figure 6A–C, lanes 9–11). In contrast, the mutations did not affect the interaction with DDX6/RCK, as expected (Figure 6D). Removing the helical protrusion (Mut-3) did not affect the PatL1 interaction with DCP2 and decapping activators (Figure 6A–C, lane 12).

To assess how the mutations affect PatL1 association with decapping complexes, we tested the activity of the mutants in decapping assays *in vitro*. In accordance with the results of the coimmunoprecipitation assay, Mut-1 and Mut-2 failed to copurify with decapping activity, whereas Mut-3 associated with decapping activity (Figure 3C and D). Taken together, these results show that the Pat-C conserved and basic patches are crucial for the interaction with DCP2, EDC4 and the LSm1–7 ring.

We next tested the ability of PatL1 mutants to localize to P-bodies. We observed that Mut-1 and Mut-2 were dispersed throughout the cytoplasm in about 90% of cells (Figure 4F and G), whereas Mut-3 accumulates in foci (Figure 4H). Furthermore, in about 60% of cells expressing Mut-1 or Mut-2, endogenous P-bodies were dispersed (Figure 4F and G), indicating that these mutants inhibit P-body formation in a dominant-negative manner.

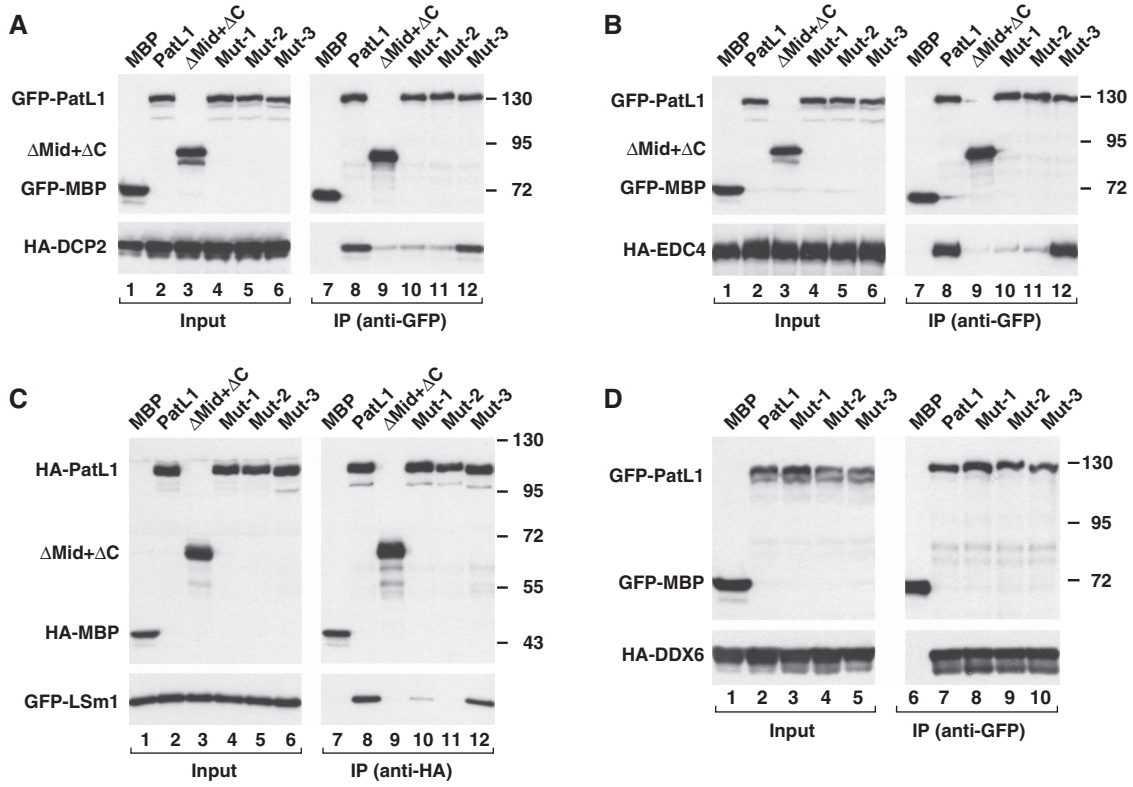

Figure 6 A basic and conserved surface on Pat-C enables PatL1 to interact with DCP2, EDC4 and the LSm1–7 ring. (**A**–**D**) GFP- and HA-tagged proteins were coexpressed in human cells as indicated. Cell lysates were immunoprecipitated using anti-GFP or anti-HA antibodies and analysed as described in Figure 1.

The Pat-C conserved surface is required for mRNA decapping in vivo

To investigate how the Pat-C conserved surface influences decapping *in vivo*, we took advantage of a complementation assay established in *D. melanogaster* S2 cells (Haas *et al*, 2010). First, we mutated conserved residues in *D. melanogaster* HPat corresponding to Mut-2 in human PatL1 (Supplementary Figure S1B) and examined whether the protein could coimmunoprecipitate LSm1 in S2 cells. Similar to results obtained with human PatL1, we found that mutating the conserved residues abrogates the interaction with LSm1 as efficiently as deleting Pat-C entirely (Figure 7A). Thus, the conserved surface on Pat-C is also required for the interaction of *D. melanogaster* HPat with LSm1–7.

Next, we investigated whether HPat Mut-2 could restore decapping and mRNA degradation in cells depleted of endogenous HPat (Haas *et al*, 2010). To monitor decapping, we used the F-Luc-5BoxB reporter, which is rapidly degraded when coexpressed with a λN fusion of the GW182 protein. Indeed, λN-GW182 triggers deadenylation of the F-Luc-5BoxB reporter, after which the mRNA is decapped and then subjected to exonucleolytic digestion (Eulalio *et al*, 2007b). Inhibiting decapping prevents GW182-mediated mRNA degradation and leads to the accumulation of deadenylated mRNA decay intermediates, which exhibit a characteristically higher electrophoretic mobility than polyadenylated transcripts (Figure 7B, lane 4 versus 2; Eulalio *et al*, 2007b). Therefore, monitoring the accumulation of the deadenylated F-Luc-5BoxB mRNA can track a block in decapping.

S2 cells were transiently transfected with three plasmids: the F-Luc-5BoxB reporter; a plasmid expressing λN-GW182 or the λN-peptide; and a transfection control plasmid, encoding *Renilla* luciferase (R-Luc). In the presence of λN-GW182 we observed that, relative to cells expressing the λN-peptide alone, the levels of the F-Luc-5BoxB mRNA were reduced five-fold (Figure 7B, lane 2 versus 1 and Figure 7C). In contrast, codepleting HPat and Me31B inhibited decapping and allowed the deadenylated F-Luc-5BoxB mRNA to accumulate (Figure 7B, lane 4 and Figure 7C).

Expressing HPat wild type in depleted cells restored decapping and degradation of F-Luc-5BoxB mRNA (Figure 7B, lane 6 and Figure 7C). As reported before, the HPat mutant lacking Pat-C was defective in promoting mRNA degradation, indicating that Pat-C is required for decapping *in vivo* (Figure 7B, lane 8; Haas *et al*, 2010). Importantly, HPat Mut-2 was completely defective in restoring decapping and therefore the deadenylated mRNA was still detectable (Figure 7B, lane 10 and Figure 7C). All proteins were expressed at comparable levels (Figure 7D). We conclude that the conserved surface on Pat-C is essential for HPat to promote mRNA decapping *in vivo*.

Discussion

In this study, we determined the structure of PatL1 C-terminal domain (Pat-C), the only domain in Pat proteins that folds independently. Pat-C folds into an α–α superhelix, exposing basic and conserved residues on one side of this domain. Our functional and structural analysis of Pat-C identified several critical and distinct functions for this protein domain: (1) it

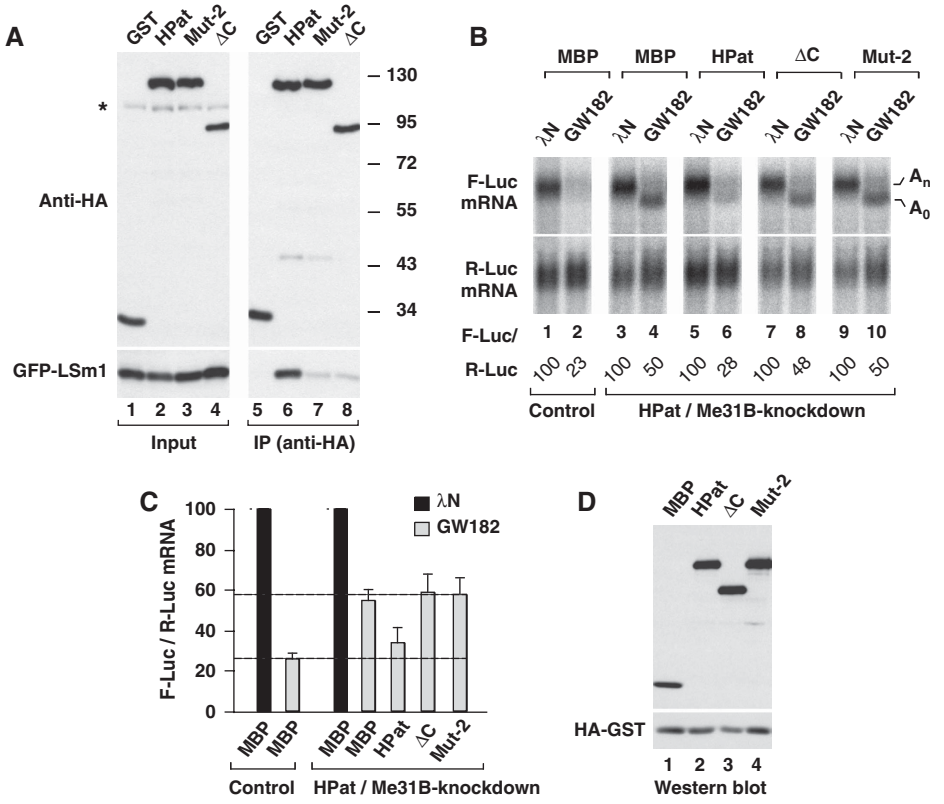

Figure 7 Pat-C is required for decapping *in vivo*. (**A**) Pat-C conserved residues are required for HPat to interact with the LSm1–7 complex. GFP- and HA-tagged proteins were coexpressed in *D. melanogaster* S2 cells as indicated. Cell lysates were immunoprecipitated using a monoclonal anti-HA antibody. HA-GST (Glutathion-S-Transferase) served as negative control. Inputs and immunoprecipitates were analysed as described in Figure 1. (**B**–**D**) Control S2 cells (treated with GFP dsRNA) or cells codepleted of HPat and Me31B were cotransfected with a mixture of three plasmids: one expressing the F-Luc-5BoxB reporter, another expressing λN-HA-GW182 or the λN-HA peptide and a third expressing *Renilla* luciferase (R-Luc). Plasmids (5 ng) expressing HA-MBP, wild-type HA-HPat, HPatΔC or Mut2 were included in the transfection mixtures, as indicated. RNA samples were analysed by northern blot. F-Luc-5BoxB mRNA levels were normalized to those of the *Renilla* luciferase. For each condition, the normalized values of F-Luc mRNA were set to 100 in the presence of the λN-HA peptide. Mean values ± s.d. for three independent experiments are shown in (**C**). (**D**) Full-length HPat and mutants were expressed at comparable levels.

mediates RNA binding through a conserved basic surface; (2) it cooperates with the P-rich region to provide a binding surface for DCP2 and EDC4; (3) it cooperates with the Mid domain to provide a high-affinity interaction with the LSm1–7 ring; (4) it is required for PatL1 to accumulate in P-bodies and (5) it is essential for mRNA decapping *in vivo*. The multiplicity of interactions mediated by Pat-C suggests that these interactions might be synergistic and antagonistic and thus may have a regulatory function as discussed below.

PatL1 interacts with DCP2 and multiple decapping activators

In this article, we show the PatL1 N-term sequence confers binding to DDX6/RCK. This interaction is conserved in *D. melanogaster* where we showed that the HPat N-term sequence also interacts with Me31B (Haas *et al*, 2010). We further show the P-rich region and Pat-C both contribute to the interaction with DCP2 and EDC4, whereas LSm1–7 binding requires the Mid domain and Pat-C (Figures 2 and 8). From our studies, we cannot conclude whether PatL1 interacts with decapping activators and DCP2 directly. Nevertheless, our results allow us to draw several conclusions. First, DCP2, EDC4 and the LSm1–7 ring interact with PatL1 independently of the conserved N-term sequence, and thus independently of DDX6/RCK. Second, EDC4 and DCP2

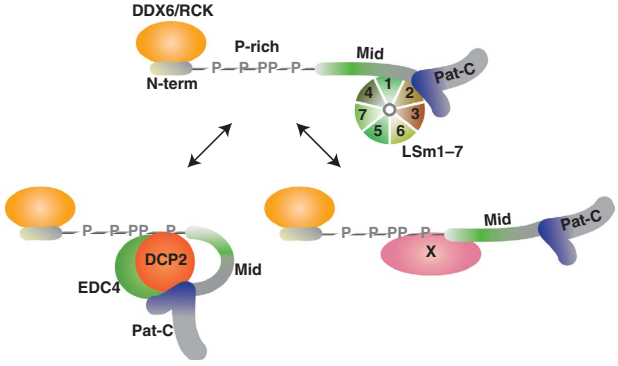

Figure 8 Model summarizing the protein interactions described in this study. PatL1 may adopt two different conformations: one with the ability to interact with LSm1–7 and the other interacting either with EDC4 and DCP2 or with an as yet unknown protein factor (X) binding to the P-rich region and blocking the accessibility of the Mid domain to the LSm1–7 ring.

interact with PatL1 independently of the LSm1–7 ring, because deleting the Mid domain abolishes LSm1–7 binding but not DCP2 or EDC4 binding. Third, LSm1–7 binding anti-correlates with the binding of EDC4/DCP2, because, if the P-rich region is fused to a protein fragment containing the

Mid domain plus Pat-C, then the affinity for LSm1–7 decreases, but binding to DCP2 and EDC4 is stimulated. Finally, binding to DCP2, EDC4 and LSm1–7 is unlikely to be entirely mediated by RNA because mutations in conserved Pat-C surface residues do not affect RNA binding but abolish the interaction with decapping factors. On the other hand, mutations in the positive Pat-C surface abolish the interaction both with RNA and with decapping factors, suggesting that RNA may contribute to the affinity of PatL1 for decapping factors.

The function of Pat-C in mRNA decapping

In this study, we show that Pat-C is required for *D. melanogaster* and human Pat proteins to interact with the LSm1–7 ring. Whether this is also true for yeast has not been directly investigated; however, indirect evidence suggests that Pat-C might also be important for LSm1 binding in yeast. Indeed, Pilkington and Parker (2008) reported that the accumulation of LSm1 in P-bodies depends on Pat1, and that LSm1 interacts with the Pat1 Mid domain. Accordingly, it is intriguing that Pat-C is necessary and sufficient to promote LSm1 accumulation in P-bodies (Pilkington and Parker, 2008). Our results provide an explanation for this, in that although the isolated Mid domain is sufficient for LSm1 binding, Pat-C is also required in the context of full-length Pat proteins and may provide a low-affinity LSm1-binding site.

Nevertheless, studies in *S. cerevisiae* indicated that for Pat1 function *in vivo* Pat-C is dispensable; whereas our studies suggest, in *D. melanogaster* and human cells, this domain is essential (Pilkington and Parker, 2008; Haas *et al*, 2010). One possible explanation for resolving the discrepancy between *S. cerevisiae* and metazoa lies in the realization that the precise composition and stoichiometry of decapping complexes differs significantly between these organisms as for example, yeast lacks an EDC4 ortholog. Thus, it is possible that for metazoa, Pat-C is essential in decapping because it interacts with EDC4 and DCP2. Yeast Pat1 interacts with DCP2 but this interaction is mediated by RNA (Tharun and Parker, 2001). The essential function of Pat-C may therefore reflect additional functions this domain acquired in metazoa.

Does Pat switch decapping partners?

An unexpected observation from our studies is that Pat-C, but not the Mid domain is sufficient for LSm1 binding in human cells, whereas in yeast and *D. melanogaster* cells, the Mid domain but not Pat-C is sufficient (Pilkington and Parker, 2008; Haas *et al*, 2010). Our hypothesis to explain these results is that Pat proteins contain two distinct LSm1-binding sites: one in the Mid domain and one in Pat-C. Human PatL1 interacts with LSm1 predominantly through Pat-C; whereas in *D. melanogaster* and *S. cerevisiae*, the interaction through the Mid domain dominates. However, for LSm1 binding, even when the interaction with the Mid domain dominates, there is a general requirement for Pat-C in the context of full-length Pat. Indeed, in addition to enhance LSm1 binding by the Mid domain, Pat-C is required to counteract a negative effect of the P-rich region. Of note, the N-terminal boundary of the Mid domain is difficult to define and this may contribute to the differences observed between species.

The requirement of Pat-C for LSm1–7 binding raises the question of whether the LSm1–7 ring competes with DCP2/EDC4 for binding to Pat-C. Two lines of evidence support this scenario: (1) as mentioned above, we observed that DCP2/EDC4- and LSm1 binding anti-correlate and (2) it is unlikely that the small conserved patch on Pat-C can bind to DCP2/EDC4 and the LSm1–7 ring simultaneously.

Competition between DCP2/EDC4 and LSm1–7 for Pat binding would also help to explain the negative effects of the P-rich region on the interaction with LSm1–7, because the P-rich region enhances the affinity of DCP2/EDC4 for PatL1. Furthermore, there may be some residual affinity of DCP2/EDC4 for the P-rich region even in the absence of Pat-C. In this case, DCP2/EDC4 could sterically mask the access of the LSm1–7 ring to the Mid domain.

Alternatively, the negative effect of the P-rich region on LSm1–7 binding could be a direct one, for example by occluding the LSm1–7 binding site on the Mid domain. However, it is difficult to conceive how two unstructured protein regions could interact with each other specifically. Consistently, we could not detect an interaction *in trans* between the P-rich region and the Mid domain. A third explanation could be that additional interacting partners bind to the P-rich region and regulate the accessibility of the Mid domain (Figure 8, factor X). Although proteins binding to the P-rich region have not yet been identified, it is likely that this region interacts with additional components of the decay machinery, because in *D. melanogaster* the P-rich region was sufficient to trigger degradation of mRNAs in tethering assays (Haas *et al*, 2010).

Regardless of precisely how the P-rich region inhibits the Mid domain from binding LSm1, our results suggest this binding could be regulated, and that Pat proteins might adopt two different conformations one with and the other without affinity for LSm1–7 (Figure 8). It remains to be established whether these conformations represent distinct complexes with specific functions or sequential steps in the assembly of active decapping complexes on target mRNAs. More generally, our findings challenge the notion that Pat proteins act as simple scaffolds for the simultaneous assembly of decapping factors and rather suggest that certain of the interactions between decapping factors may occur sequentially allowing decapping complexes to assemble in a stepwise manner.

Materials and methods

Protein expression, purification and crystallization

Human PatL1 proteins were expressed with an N-terminal His_6-tag in the *Escherichia coli* strain BL21 (DE3) or BL21 Star (DE3; Invitrogen) at 25°C overnight. After purification by an Ni^{2+}-affinity step (HiTrap Chelating HP column, GE Healthcare), the His_6-tag was cleaved with PreScission protease. The proteins were further purified by ion exchange chromatography and gel filtration (HiTrap SP HP and HiLoad 26/60 Superdex 75 columns, GE Healthcare). A detailed description of the crystallization procedures is provided in the Supplementary data.

Structure determination and refinement

Diffraction data were collected on beamline X10SA of the Swiss Light Source, Villigen, Switzerland. The structure of the human PatL1 fragment, Pat-C-Δloop (Form I), was determined from multiple-wavelength anomalous dispersion data, collected on a crystal of selenomethionine-substituted protein. For Pat-C (Form II) and Pat-C-Δloop with bound sulphate (Form III), the structures were solved by molecular replacement using Pat-C-Δloop (Form I) as search model. Additional information is provided in the Supplementary data.

DNA constructs

Plasmids for expressing DCP2, DDX6/RCK and EDC4 in human cells were described before (Tritschler *et al*, 2009a, b). Plasmids for expressing PatL1 were generated by cloning the corresponding cDNA into the pEGFP-C1 vector (Clontech) or the pλN-HA-C1 vector (Tritschler *et al*, 2009a, b). Human LSm1 was cloned between the XhoI and EcoR1 sites of the pλN-HA-C1 vector. PatL1 mutants were generated by site-directed mutagenesis using the QuickChange mutagenesis kit from Stratagene and the appropriate oligonucleotide sequences.

Coimmunoprecipitation assays, western blotting and fluorescence microscopy

For coimmunoprecipitation assays, HEK-293 cells were grown in 10 cm plates and transfected using Lipofectamine 2000 (Invitrogen). The transfection mixtures contained 7 μg of the GFP and HA constructs. For fluorescence microscopy, human HeLa cells were grown on coverslips in 24-well plates and transfected using Lipofectamine 2000 (Invitrogen). The transfection mixtures contained 0.3 μg of plasmids expressing GFP-protein fusions. Cells were collected 2 days after transfection. Coimmunoprecipitations, western blotting and fluorescence microscopy were performed as described earlier (Tritschler *et al*, 2009b). Additional information is provided in the Supplementary data.

Decapping assays

Decapping assays were performed as described earlier (Lykke-Andersen, 2002; Tritschler *et al*, 2009b), using an *in vitro* synthesized RNA (127 nucleotides). The RNA probe was labelled with [α-^{32}P]GTP using the ScriptCap m^{7}G Capping System and the ScriptCap 2′-O-Methyltransferase kit (EPICENTRE Biotechnologies). Reactions were stopped by adding up to 50 mM EDTA and analysed on PEI cellulose thin-layer chromatography plates (Merck) in 0.75 M LiCl (1 μl/sample). Unlabelled GDP, m^{7}GMP, m^{7}GDP and m^{7}GTP were used as markers.

Immunoprecipitations, RNA interference and complementation assay in D. melanogaster S2 cells

Protein coimmunoprecipitations and complementation in S2 cells were performed as described earlier (Haas *et al*, 2010). Mutants of *D. melanogaster* HPat were generated by site-directed mutagenesis using the plasmid pAc5.1B-HA-HPat (dsRNA resistant) as template, and the QuickChange mutagenesis kit from Stratagene. Transfections of S2 cells were performed in six-well plates, using Effectene transfection reagent (Qiagen). Firefly and *Renilla* luciferase activities were measured 3 days after transfection using the Dual-Luciferase Reporter Assay System (Promega). Total RNA was isolated using TriFast (Peqlab Biotechnologies) and analysed as described earlier (Haas *et al*, 2010).

Coordinate deposition

Coordinates of the human PatL1 C-terminal domain constructs Pat-C-Δloop (Form I), Pat-C (Form II) and Pat-C-Δloop with bound sulphate (Form III) have been deposited in the Protein Data Bank under accession numbers 2xes, 2xeq and 2xer, respectively.

Supplementary data

Supplementary data are available at *The EMBO Journal* Online (http://www.embojournal.org).

Acknowledgements

We are grateful to R Büttner, M Fauser and S Helms for excellent technical assistance. We thank the staff at the PX beamlines of the Swiss Light Source for assistance with data collection. This study was supported by the Max Planck Society, by grants from the Deutsche Forschungsgemeinschaft (DFG, FOR855 and the Gottfried Wilhelm Leibniz Program awarded to EI), and by the Sixth Framework Programme of the European Commission through the SIROCCO Integrated Project LSHG-CT-2006-037900. OW held a personal VIDI fellowship from the Dutch National Science Organization (NWO-VIDI, CW 700.54.427).

Conflict of interest

The authors declare that they have no conflict of interest.

References

Bail S, Kiledjian M (2006) More than 1 + 2 in mRNA decapping. *Nat Struct Mol Biol* **13:** 7–9

Bonnerot C, Boeck R, Lapeyre B (2000) The two proteins Pat1p (Mrt1p) and Spb8p interact *in vivo*, are required for mRNA decay, and are functionally linked to Pab1p. *Mol Cell Biol* **20:** 5939–5946

Bouveret E, Rigaut G, Shevchenko A, Wilm M, Seraphin B (2000) A Sm-like protein complex that participates in mRNA degradation. *EMBO J* **19:** 1661–1671

Chowdhury A, Mukhopadhyay J, Tharun S (2007) The decapping activator Lsm1p-7p-Pat1p complex has the intrinsic ability to distinguish between oligoadenylated and polyadenylated RNAs. *RNA* **13:** 998–1016

Chowdhury A, Tharun S (2008) lsm1 mutations impairing the ability of the Lsm1p-7p-Pat1p complex to preferentially bind to oligoadenylated RNA affect mRNA decay *in vivo*. *RNA* **14:** 2149–2158

Chowdhury A, Tharun S (2009) Activation of decapping involves binding of the mRNA and facilitation of the post-binding steps by the Lsm1-7-Pat1 complex. *RNA* **15:** 1837–1848

Coller JM, Tucker M, Sheth U, Valencia-Sanchez MA, Parker R (2001) The DEAD box helicase, Dhh1p, functions in mRNA decapping and interacts with both the decapping and deadenylase complexes. *RNA* **7:** 1717–1727

Edwards TA, Pyle SE, Wharton RP, Aggarwal AK (2001) Structure of Pumilio reveals similarity between RNA and peptide binding motifs. *Cell* **105:** 281–289

Eulalio A, Behm-Ansmant I, Schweizer D, Izaurralde E (2007a) P-body formation is a consequence, not the cause of RNA-mediated gene silencing. *Mol Cell Biol* **27:** 3970–3981

Eulalio A, Rehwinkel J, Stricker M, Huntzinger E, Yang S-F, Doerks T, Dorner S, Bork P, Boutros M, Izaurralde E (2007b) Target-specific requirements for enhancers of decapping in miRNA-mediated gene silencing. *Genes Dev* **21:** 2558–2570

Fenger-Grøn M, Fillman C, Norrild B, Lykke-Andersen J (2005) Multiple processing body factors and the ARE binding protein TTP activate mRNA decapping. *Mol Cell* **20:** 905–915

Fischer N, Weis K (2002) The DEAD box protein Dhh1 stimulates the decapping enzyme Dcp1. *EMBO J* **21:** 2788–2797

Franks TM, Lykke-Andersen J (2008) The control of mRNA decapping and P-body formation. *Mol Cell* **32:** 605–615

Fromont-Racine M, Mayes AE, Brunet-Simon A, Rain JC, Colley A, Dix I, Decourty L, Joly N, Ricard F, Beggs JD, Legrain P (2000) Genome-wide protein interaction screens reveal functional networks involving Sm-like proteins. *Yeast* **17:** 95–110

Haas G, Braun JE, Igreja C, Tritschler F, Nishihara T, Izaurralde E (2010) HPat provides a link between deadenylation and decapping in metazoa. *J Cell Biol* **189:** 289–302

Hatfield L, Beelman CA, Stevens A, Parker R (1996) Mutations in trans-acting factors affecting mRNA decapping in *Saccharomyces cerevisiae*. *Mol Cell Biol* **16:** 5830–5838

He W, Parker R (2001) The yeast cytoplasmic LsmI/Pat1p complex protects mRNA 3′ termini from partial degradation. *Genetics* **158:** 1445–1455

Holm L, Sander C (1995) Dali: a network tool for protein structure comparison. *Trends Biochem Sci* **20:** 478–480

Huber AH, Nelson WJ, Weis WI (1997) Three-dimensional structure of the armadillo repeat region of beta-catenin. *Cell* **90:** 871–882

Jínek M, Eulalio A, Lingel A, Helms S, Conti E, Izaurralde E (2008) The C-terminal region of Ge-1 presents conserved structural features required for P-body localization. *RNA* **14:** 1991–1998

Kedersha N, Anderson P (2007) Mammalian stress granules and processing bodies. *Methods Enzymol* **431:** 61–81

Lykke-Andersen J (2002) Identification of a human decapping complex associated with hUpf proteins in nonsense-mediated decay. *Mol Cell Biol* **22:** 8114–8121

Matsuura Y, Stewart M (2004) Structural basis for the assembly of a nuclear export complex. *Nature* **432:** 872–877

Murzin AG, Brenner SE, Hubbard T, Chothia C (1995) SCOP: a structural classification of proteins database for the investigation of sequences and structures. *J Mol Biol* **247:** 536–540

Pilkington GR, Parker R (2008) Pat1 contains distinct functional domains that promote P-body assembly and activation of decapping. *Mol Cell Biol* **28:** 1298–1312

Scheller N, Resa-Infante P, de la Luna S, Galao RP, Albrecht M, Kaestner L, Lipp P, Lengauer T, Meyerhans A, Díez J (2007) Identification of PatL1, a human homolog to yeast P body component Pat1. *Biochim Biophys Acta* **1773:** 1786–1792

Simon E, Camier S, Séraphin B (2006) New insights into the control of mRNA decapping. *Trends Biochem Sci* **31:** 241–243

Tharun S (2009) Lsm1-7-Pat1 complex: a link between 3′ and 5′-ends in mRNA decay? *RNA Biol* **6:** 228–232

Tharun S, He W, Mayes AE, Lennertz P, Beggs JD, Parker R (2000) Yeast Sm-like proteins function in mRNA decapping and decay. *Nature* **404:** 515–518

Tharun S, Parker R (2001) Targeting an mRNA for decapping: displacement of translation factors and association of the Lsm1p-7p complex on deadenylated yeast mRNAs. *Mol Cell* **8:** 1075–1083

Tritschler F, Braun JE, Eulalio A, Truffault V, Izaurralde E, Weichenrieder O (2009a) Structural basis for the mutually exclusive anchoring of P-body components EDC3 and Tral to the DEAD-box protein DDX6/Me31B. *Mol Cell* **33:** 661–668

Tritschler F, Braun JE, Motz C, Igreja C, Haas G, Truffault V, Izaurralde E, Weichenrieder O (2009b) DCP1 forms asymmetric trimers to assemble into active mRNA decapping complexes in metazoa. *Proc Natl Acad Sci USA* **106:** 21591–21596

van Dijk E, Cougot N, Meyer S, Babajko S, Wahle E, Séraphin B (2002) Human Dcp2: a catalytically active mRNA decapping enzyme located in specific cytoplasmic structures. *EMBO J* **21:** 6915–6924

Wang X, McLachlan J, Zamore PD, Hall TM (2002) Modular recognition of RNA by a human pumilio-homology domain. *Cell* **110:** 501–512

